Evidence for deep groundwater flow and convective heat transport in mountainous terrain, Delta County, Colorado, USA

Gregory D. Lazear

Abstract The Tongue Creek watershed lies on the south flank of Grand Mesa in western Colorado, USA and is a site with 1.5 km of topographic relief, heat flow of 100 mW/m^2, thermal conductivity of 3.3 W m^{-1} °C^{-1}, hydraulic conductivity of 10^{-8} m/s, a water table that closely follows surface topography, and groundwater temperatures 3–15°C above mean surface temperatures. These data suggest that convective heat transport by groundwater flow has modified the thermal regime of the site. Steady state three-dimensional numerical simulations of heat flow, groundwater flow, and convective transport were used to model these thermal and hydrological data. The simulations provided estimates for the scale of hydraulic conductivity and bedrock base flow discharge within the watershed. The numerical models show that (1) complex three-dimensional flow systems develop with a range of scales from tens of meters to tens of kilometers; (2) mapped springs are frequently found at locations where contours of hydraulic head indicate strong vertical flow at the water table, and; (3) the distribution of groundwater temperatures in water wells as a function of surface elevation is predicted by the model.

Résumé Le bassin-versant de Tongue Creek s'étend sur le flanc sud de la Grande Mesa dans l'Ouest du Colorado, USA; c'est un site présentant 1.5 km de relief topographique, une circulation de chaleur de 100 mW/m^2, une conductivité thermique de 3.3 W m^{-1} °C^{-1}, et une conductivité hydraulique de 10^{-8} m/s, une nappe suivant assez bien la surface topographique, et une température des eaux souterraines comprise entre 3 et 15°C au dessus de la température moyenne en surface. Ces données suggèrent que le transport convectif de chaleur via l'écoulement des eaux souterraines, a modifié le régime thermique du site. Des simulations numériques du transport de chaleur, de l'écoulement des eaux souterraines et du transport convectif ont été utilisées ces données thermiques et hydrologiques. Ces simulations ont apporté des estimations quant à l'échelle des conductivités hydrauliques et l'écoulement de base au sein du bassin-versant. Le modèle numérique montre que (1) les systèmes complexes d'écoulement tridimensionnel étendent des perméabilités comprises entre plusieurs dizaines de mètres jusqu'à plusieurs dizaines de kilomètres, (2) les sources cartographiées sont fréquemment localisées là où la piézométrie indique généralement des écoulements verticaux forts, et (3) la distribution de la température des eaux souterraines dans les puits, en tant que fonction de l'altitude, est prédite par le modèle.

Resumen La cuenca del arroyo Tongue queda en el costado sur de la Gran Mesa, en la parte occidental de Colorado, EE.UU. Es un sitio con 1.5 km de relieve topográfico, un flujo de calor de 100 mW/m^2, una conductividad térmica de 3.3 W m^{-1} °C^{-1}, conductividad hidráulica de 10^{-8} m/s, un nivel freático que sigue estrechamente a la superficie topográfica, y temperaturas del agua subterránea que están entre 3–15°C sobre las temperaturas medias de superficie. Estos datos sugieren que el transporte convectivo de calor, debido al flujo de agua subterránea ha modificado el régimen térmico del sitio. Las simulaciones numéricas tridimensionales en condiciones estacionarias de flujo de calor, flujo de agua subterránea, y transporte convectivo, se usaron para modelar estos datos térmicos e hidrológicos. Las simulaciones proporcionan estimativos para el nivel de conductividad hidráulica y para la descarga de flujo base desde el lecho rocoso dentro de la cuenca. Los modelos numéricos muestran que: (1) los sistemas de flujo tridimensionales complejos, se desarrollan con un rango de tamaño variando entre decenas de metros a decenas de kilómetros; (2) Los manantiales cartografiados se encuentran con frecuencia en situaciones dónde los contornos de cabeza hidráulica indican un flujo vertical fuerte en el nivel freático, y (3) La distribución de temperaturas del agua subterránea en los pozos de agua, son predichas por el modelo en función de la elevación de la superficie.

Keywords Mountainous terrain · Groundwater flow · Convection · Heat flow · Springs

Received: 31 May 2005 / Accepted: 14 April 2006
Published online: 18 July 2006

G. D. Lazear (✉)
20508 Brimstone Rd., Cedaredge,
CO, USA
e-mail: gdlazear@tds.net
Tel.: +1-970-8566810

 DOI 10.1007/s10040-006-0058-8

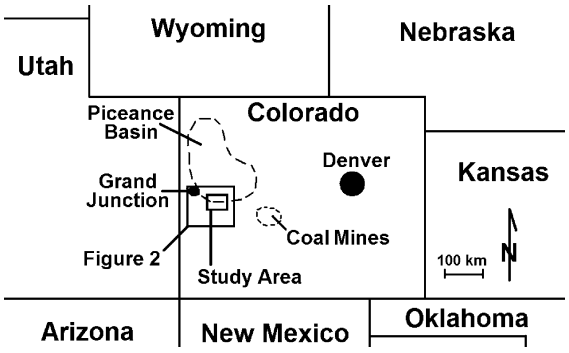

Fig. 1 Location of the study area in west-central Colorado, USA, and proximity of the Piceance Basin to the north, and coal mining areas to the east

Introduction

The transport of heat by forced convection of groundwater and the resulting modification of the subsurface thermal regime have been well documented in the literature, both theoretically (Domenico and Palciauskas 1973; Smith and Chapman 1983; Forster and Smith 1989) and in case studies (Woodbury and Smith 1988; Deming 1993; Manga and Kirchner 2004). A review of the field of heat as a groundwater tracer was recently published by Anderson (2005). Previous work has used two-dimensional numerical modeling to provide insight and to aid in the interpretation of field data. The study presented here combines thermal data with steady state three-dimensional numerical simulation of groundwater flow to constrain the scale of hydraulic conductivity and the base flow discharge within a watershed. Thermal data provide a redundancy that allows estimation of unknown hydraulic conductivity (Woodbury and Smith 1988).

The site for this study is a single watershed on the south flank of Grand Mesa in the vicinity of Cedaredge, Colorado. Figure 1 depicts the location within the US, and Fig. 2 shows the topographic setting. The mesa rises nearly 2 km above the surrounding countryside to an elevation of 3,350 m above sea level (m a.s.l.), and was formed when Miocene basalt flows created a 200-m-thick cap rock over a sequence of soft Tertiary and Cretaceous strata, thereby armoring them against erosion. In the intervening 10 million years, a combination of regional uplift and erosion of the soft strata along the margins of the basalt has produced the striking mesa seen today (Young and Young 1977; Cole and Sexton 1981; Dethier 2001).

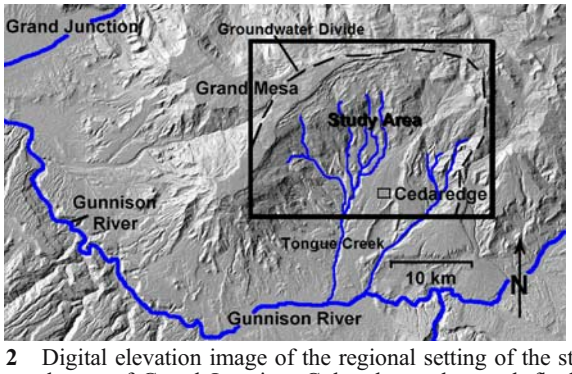

Fig. 2 Digital elevation image of the regional setting of the study area south-east of Grand Junction, Colorado on the south flank of Grand Mesa. Topographic data is from USGS digital elevation models

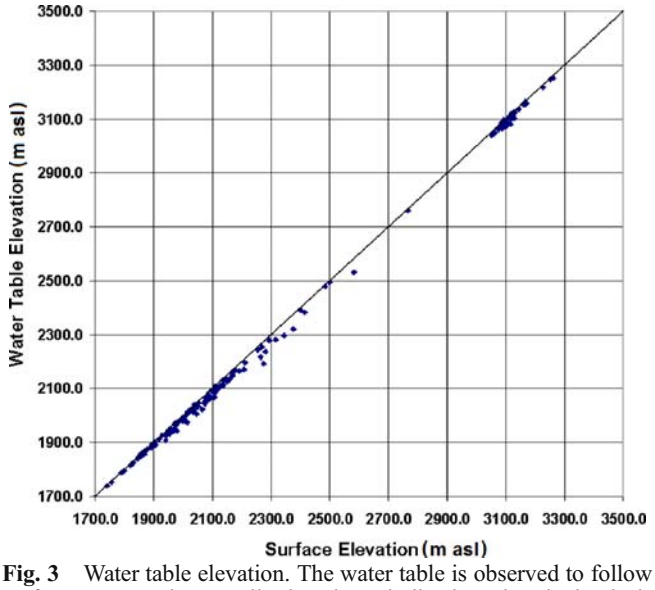

Fig. 3 Water table elevation. The water table is observed to follow surface topography at all elevations indicating that bedrock is saturated. Data are from water well records of the Colorado State Engineers Office

The study area has a number of features of hydrological interest including high precipitation, shallow water table, high heat flow, and low hydraulic conductivity. Precipitation as a function of elevation ranges from about 0.18 m/year at low elevation (1,370 m a.s.l.) to 1 m/year at high

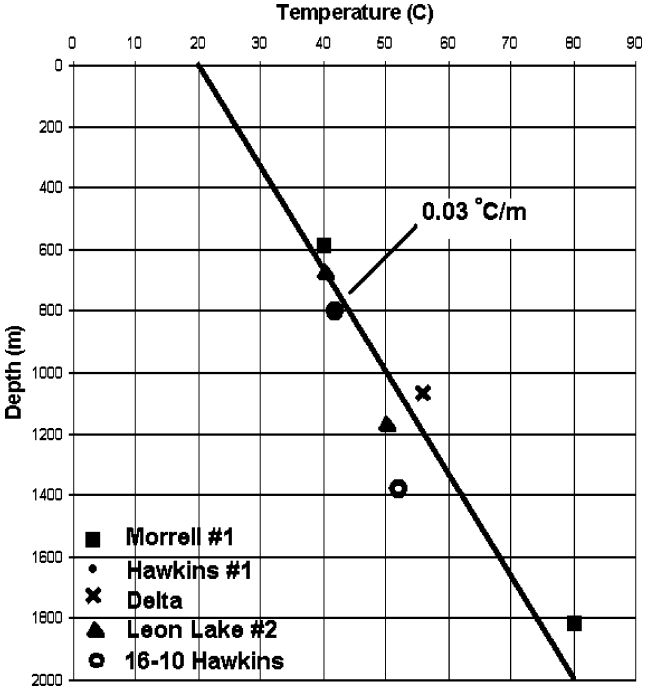

Fig. 4 Average thermal gradient estimated from local oil and gas wells

DOI 10.1007/s10040-006-0058-8

Table 1 Spring and well water data

Site_name	West longitude	North latitude	Type	SC (uS/cm)	Temperature (C)	Elevation (m a.s.l.)	X-grid	Y-grid
SC01109431CDC1[a]	107.9417	39.04806	Well	446	7	3,110	94	142
SC01109431DCC1[a]	107.9369	39.04917	Well	173	5	3,110	96	143
SC01209503DBD1[a]	107.9931	39.03472	Spring	61	10	3,067	67	131
SC01209509AAB1[a]	108.0086	39.03139	Well	83	3.5		59	129
SC01209515ACC1[a]	107.995	39.01167	Spring	103	3	2,951	66	112
SC01309308BAC1[a]	107.8114	38.94222	Well	5,390	10	2,122	160	55
SC01309316AAD[a]	107.7811	38.92861	Well	1,480	12	2,280	176	44
SC01309401ACC1[a]	107.8447	38.9525	Well	1,060	12.5	2,256	143	64
SC01309406BAC1[a]	107.9439	38.95556	Well	325	12.5	2,134	92	66
SC01309409ADB1[a]	107.8881	38.94083	Well	830	13.5	2,133	121	54
SC01309415AAB1[a]	107.8803	38.92944	Well	780	16	2,183	125	45
SC01309418DBA1[a]	107.9394	38.925	Well	325	12	1,963	95	41
SC01309511ACC1[a]	107.9792	38.93833	Well	930	13.5	1,976	74	52
SC01309511CAD1[a]	107.9828	38.93667	Well	1,230	13.5	1,970	73	51
SC01309511CBA1[a]	107.9847	38.93806	Well	1,120	15.5	1,994	72	52
SC01309511CCB1[a]	107.9869	38.93333	Well	2,090	16.5	2,043	70	48
SC01309512ACC1[a]	107.9594	38.93806	Well	626	14	2,003	85	52
SC01309512BDC1[a]	107.9622	38.93667	Well	680	15.5	1,963	83	51
SC01309512BDC2[a]	107.9622	38.93667	Well	1,850	16	1,963	83	51
SC01309512BDC3[a]	107.9622	38.93667	Well	3,820	14	1,963	83	51
SC01309512CAA1[a]	107.9597	38.9375	Well	1,150	15.5	1,921	84	51
SC01309517AAD1[a]	108.0292	38.92694	Well	1,330	14	2,061	49	43
SC01309624ACC1[a]	108.0733	38.90944	Well	1,360	15	2,366	26	28
SC01309625BDC1[a]	108.0775	38.89333	Well	1,110	15.5	2,250	24	15
SP-CD01[b]	107.9578	38.92917	Spring	711	15.1	1,930	85	45
SP-CD02[b]	107.95	38.925	Spring	643	9.98	1,979	89	41
SP-CD03[b]	107.9425	38.92556	Spring	747	9.58	1,951	93	42
SP-DW02[b]	107.9817	38.93139	Well	571	14.6	1,963	73	46
SP-DW03[b]	107.8625	38.98444	Well	706	9.7	2,515	134	90
SP-DW04[b]	107.9867	38.94444	Well	393	13.3	2,030	71	57
SP-DW05[b]	107.8683	38.98417	Well	475	16.2	2,509	131	90
SP-DW06[b]	107.9767	38.93694	Well	465	13.8	1,973	76	51
SP-DW07[b]	107.8844	38.95639	Well	574	16	2,276	123	67
SP-DW09[b]	107.8697	38.98028	Well	324	12	2,457	130	87
SP-DW10[b]	107.96	38.93806	Well	505	20.4	1,980	84	52
SP-PDS01[b]	107.9178	38.89972	Spring	363	15.82	1,899	106	20
SP-SG02[b]	107.8758	38.94639	Spring	529	14.6	2,335	127	59
SP-SG03[b]	107.8531	39.04083	Spring	51	20.55	2,931	139	136
SP-SG04[b]	107.7842	39.04056	Spring	29	4	3,136	174	136
SP-SG05[b]	107.7744	39.03694	Spring	42	13	3,230	179	133
SP-SG06[b]	107.7875	39.03944	Spring	41	3.9	3,099	172	135
SP-SG07[b]	107.7861	39.04194	Spring	44	5.7	3,101	173	137
SP-SG08[b]	107.7881	39.04889	Spring	33	4.1	3,153	172	143
SP-SG09[b]	107.7833	39.01333	Spring	31	3.4	3,154	174	114
SP-SG10[b]	107.8344	39.05556	Spring	43	15.2	3,096	148	148
SP-SG11[b]	107.845	39.04833	Spring	67	3.8	3,030	143	142
SP-SG12[b]	107.9622	38.93944	Spring	500	19.05	1,993	83	53
SP-SG13[b]	107.9194	38.89889	Spring	524	16.6	1,893	105	20
SP-SG16[b]	108.0086	39.00667	Spring	105	6.54	3,047	59	108
SP-SG17[b]	107.9975	39.00556	Spring	131	7.44	2,959	65	107
SP-SG18[b]	107.9975	39.01139	Spring	83	4.63	2,970	65	112
SP-SG19[b]	107.9939	39.01722	Spring	157	5.26	3,003	67	117
SP-SG20[b]	108.0008	39.02694	Spring	77	4.8	3,029	63	125
SP-SG22[b]	107.9961	39.03167	Spring	52	6.27	3,059	66	129
SP-SG23[b]	107.9942	39.03472	Spring	53	7.22	3,080	67	131
SP-SG24[b]	107.9936	39.035	Spring	53	8.96	3,084	67	132
SP-SG25[b]	107.8383	39.05861	Spring	72	8.76	3,127	146	151
SP-SG26[b]	108.0008	38.99556	Spring	86	6.18	2,965	63	99
SP-SG27[b]	108.0036	39.02167	Spring	96	4.6	3,012	62	121
SP-SG28[b]	108.0036	39.02167	Spring	95	5.31	3,009	62	121
SP-SG29[b]	108.0031	39.02278	Spring	104	5.07	3,011	62	121
SP-SG30[b]	108.0158	39.02056	Spring	78	3.18	3,110	56	120
SP-SG32[b]	107.9544	38.94028	Spring	1,160	1.89	2,006	87	54
SP-SG33[b]	107.9525	38.92944	Spring	868	9.77	1,918	88	45
SP-SG34[b]	107.9531	38.92917	Spring	905	9.63	1,919	88	45
SP-SG37[b]	107.9558	38.93444	Spring	906	9.38	1,959	86	49

 DOI 10.1007/s10040-006-0058-8

Table 1 (continued)

Site_name	West longitude	North latitude	Type	SC (uS/cm)	Temperature (C)	Elevation (m a.s.l.)	X-grid	Y-grid
SP-SG38[b]	107.9533	38.92444	Spring	718	8.8	1,906	88	41
DC-SG05[b]	108.0058	38.92722	Spring	1,360	1.46	1,917	61	43
DC-SG06[b]	107.8237	38.90297	Spring	6,390	6.69	1,954	154	23
DC-SG07[b]	107.811	38.92131	Spring	1,820	9.44	2,129	160	38
DC-SG08[b]	107.8085	38.9485	Spring	7,470	−0.46[d]	2,189	162	60
LL-PDS01[b]	107.84	39.01278	Pond	118	6.81	2,744	146	113
LL-SG01[b]	107.86	39.01306	Spring	126	9.96	2,710	135	113
LL-SG03[b]	107.8606	39.01397	Spring	107	12.65	2,718	135	114
WS-23[c]	107.9284	38.9387	Spring	580	16.2		100	52
WS-39[c]	107.9689	38.91297	Spring	994	20.1		80	31
WS-40[c]	107.9365	39.04883	Spring	59	8		96	143
WS-41[c]	107.9372	39.04933	Spring	56	11	3,049	96	143
WS-44[c]	107.952	38.93022	Spring	764	15.5	1,951	88	45
WS-46[c]	107.9514	38.93052	Spring	819	14	1,951	89	46
WS-48[c]	107.9511	38.93083	Spring	938	14		89	46
WS-55[c]	107.9479	38.93435	Spring	966	15		90	49
WS-57[c]	107.9474	38.9351	Spring	616	14		91	49
WS-58[c]	107.9467	38.93543	Spring	543	12		91	50
WS-60[c]	107.9523	38.92977	Spring	865	12		88	45
WS-62[c]	107.9526	38.9296	Spring	856	13		88	45
WS-64[c]	107.953	38.92912	Spring	1,012	13	1,951	88	44
WS-69[c]	107.9387	38.93162	Spring	770	13.4		95	47
WS-71[c]	107.9274	38.94003	Spring	552	11.7		101	53
WS-72[c]	107.9274	38.93975	Spring	534	11		101	53
WS-73[c]	107.9356	38.94462	Spring	607	13		97	57
WS-74[c]	107.9362	38.94463	Spring	444	13.8		96	57
WS-77[c]	107.9441	38.92285	Spring	699	10.5		92	39
WS-78[c]	107.9459	38.92275	Spring	920	11		91	39
WS-111 [c]	107.8148	38.91878	Spring	4,968	6	1,829	158	36
WS-132[c]	108.0056	38.9273	Spring	1,288	9		61	43
WS-133[c]	107.996	38.91375	Spring	1,138	11		66	32
WS-135[c]	107.8273	38.94912	Spring	2,668	2.2		152	61
WS-146[c]	107.8432	38.90973	Spring	819	2		144	29
WS-149[c]	107.9545	38.94033	Spring	1,122	5		87	54
WS-150[c]	107.9551	38.94018	Spring	1,025	3.8		87	54
WS-151[c]	107.9546	38.9368	Well	1,405	14.2		87	51
WS-153[c]	107.9287	38.88297	Spring	405	2.8		100	7
WS-166[c]	107.9622	38.96525	Well	830	21.3		83	74
WS-168[c]	107.9835	38.93632	Well	847	12.3		72	50
WS-169[c]	107.9854	38.93785	Well	1,000	11.4		71	52
WS-170[c]	107.9798	38.93848	Well	760	9		74	52
WS-171[c]	107.9846	38.94102	Well	1,370	18.6		72	54
WS-172[c]	107.9803	38.93872	Well	720	11.4		74	52
WS-173[c]	107.9746	38.9484	Well	495	14.8		77	60
WS-174[c]	107.987	38.94498	Well	457	17.2		70	58
WS-175[c]	107.9773	38.94388	Well	480	18		75	57
WS-176[c]	107.9878	38.94755	Well	385	15.4		70	60
WS-177[c]	107.9887	38.948	Well	335	16.5		70	60
WS-183[c]	108.0329	38.93248	Spring	1,085	12.8	2,134	47	47
WS-184[c]	108.0351	38.92782	Spring	1,973	12.7	2,152	46	43
WS-185[c]	108.061	38.9485	Spring	1,754	9.3	2,470	33	60
WS-187[c]	108.0607	38.9666	Spring	157	8	2,692	33	75
WS-189[c]	108.034	38.97742	Spring	426	11.5	2,774	46	84
WS-190[c]	108.0314	38.97478	Spring	495	7.5	2,707	48	82
WS-191[c]	108.0237	38.97547	Spring	497	13.5	2,707	52	83
WS-192[c]	108.0045	38.97603	Spring	192	9.7	2,610	62	83
WS-193[c]	107.9685	38.97747	Spring	600	8.6	2,384	80	84
WS-202[c]	107.9741	38.9287	Well	600	11.3		77	44

[a] Data from US Geological Survey (Brooks and Ackerman 1985)

[b] Data from baseline water survey for Gunnison Energy Corporation by Cordilleran Compliance Services, Inc., 2002, personal communication

[c] Data collected by the author

[d] High saline content of this water prevented freezing

 DOI 10.1007/s10040-006-0058-8

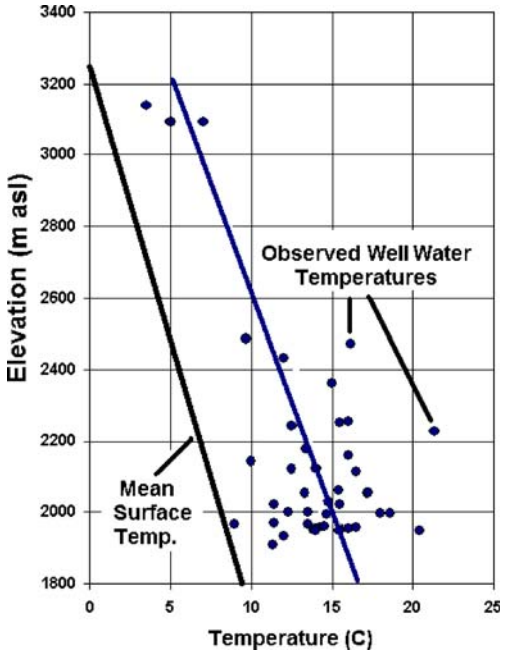

Fig. 5 Distribution of groundwater temperature with elevation measured in water wells. Observed groundwater temperatures are 2–15°C warmer than the mean annual surface temperature (*black line*) based upon climate records from Cedaredge, Colorado. Lapse rate for surface temperature is −6.5°C/km of elevation. The wide scatter in observed temperatures is thought to result from a variety of flow paths and depths of penetration at a given elevation

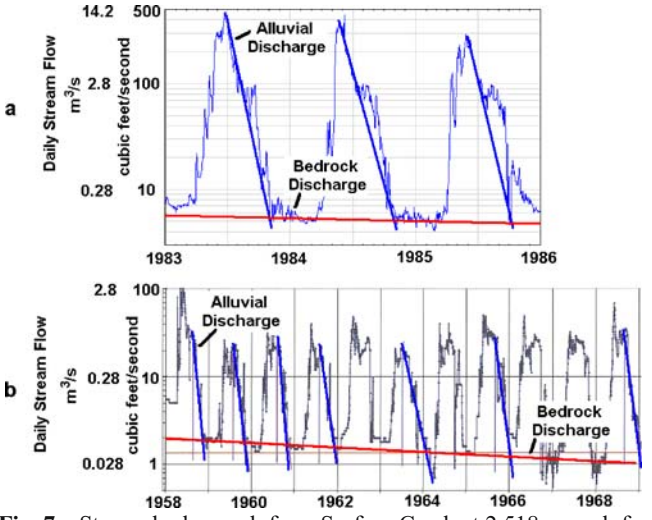

Fig. 7 Stream hydrograph for **a** Surface Creek at 2,518 m a.s.l. for the years 1983 through 1985, and **b** Ward Creek at 2,466 m a.s.l. over an 11-year period from 1958 through 1968. Steep slopes (*blue*) are alluvial discharge, while the flat segments (*red*) represent bedrock discharge. The *red lines* indicate variations in bedrock discharge

elevation (3,350 m a.s.l.). The area of the watershed within the study area is approximately 6×10^8 m^2. Assuming a linear dependence of precipitation with elevation, the total precipitation flux integrated over the watershed is equal to 15 m^3/s. Half of this precipitation falls in the upper one quarter of the elevation range (above 2,835 m a.s.l.).

Low hydraulic conductivity and high precipitation produce a shallow water table that follows surface topography. Records of domestic water wells from the Colorado State Engineers Office show that static water levels lie within 100 m of the ground surface at all elevations. These data are shown in Fig. 3. Based upon these data, the water table is assumed to follow surface topography throughout the watershed. Elevation changes in the water table of 1,500 m within the site produce strong hydraulic gradients and deep groundwater flow

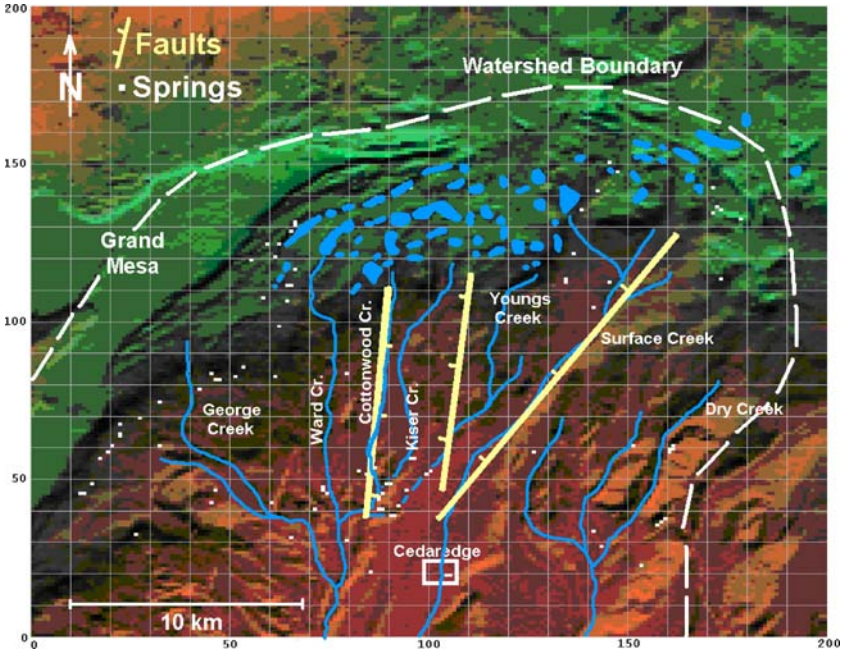

Fig. 6 Base map of the study area. The town of Cedaredge is bottom center at an elevation of 1,830 m a.s.l., and the top of Grand Mesa reaches a maximum elevation of 3,350 m a.s.l. The five drainages from George Creek to Surface Creek merge south of this map to form Tongue Creek. *Grid coordinates* are finite-difference cell numbers

 DOI 10.1007/s10040-006-0058-8

Table 2 Analysis of stream hydrographs for tributaries of Tongue Creek

Drainage	Gauge elevation. (m a.s.l.)	Drainage area (m^2)	Bedrock base flow (m^3/s)
Surface Creek	2,518	7.1×10^7	0.18
George Creek	2,213	2.7×10^7	0.028
Kiser Creek	2,430	2.8×10^7	0.021
Youngs Creek	2,183	2.7×10^7	0.034
Ward Creek	2,466	3.2×10^7	0.048
Total average	2,362	18.5×10^7	0.3

Table 4 Specification of the layered model

Hydrogeologic unit	X-grid	Y-grid	Z-grid	Strike (deg)	Dip (deg)	Hydraulic conductivity (m/s)
Tertiary	80	42	73	−90	3	10^{-8}
Upper Mesaverde	80	42	56	−90	3	2×10^{-8}
Lower Mesaverde	80	42	51	−90	3	5×10^{-8}
Mancos shale	80	42	0	0	0	10^{-9}

Grid coordinates are a point on the lower boundary plane for each hydrogeologic unit, and planes have the given strike and dip. Dip is according to the right-hand rule

with a range of scale from hundreds of meters to tens of kilometers, consistent with Toth (1962, 1963) and Domenico and Palciauskas (1973).

The study area lies in a region with heat flow of 100 mW/m^2 (SMU Geothermal Lab Website 2004). Temperature measurements shown in Fig. 4 from local deep oil and gas wells yield a thermal gradient of 30°C/km. This is in good agreement with a thermal gradient map from the SMU Geothermal Lab, and it is consistent with a thermal conductivity for the site of 3.3 $W\ m^{-1}\ °C^{-1}$ based upon rock type and saturation (Clauser and Huenges 1995). High heat flow and deep groundwater flow provide a setting in which convective heat transport can significantly modify the thermal regime of the study area. Groundwater temperatures measured in springs and water wells range from 3–15°C above the mean surface temperature as a function of elevation. Spring temperatures appear to have been influenced to some degree by the ambient temperature at the time of measurement, so this study relies upon temperatures from shallow water wells as the source of thermal data. The temperature data are listed in Table 1 and displayed in Fig. 5, along with a line representing the mean surface temperature as a function of elevation. This line was determined from mean daily temperature records for Cedaredge, Colorado, USA from 1977 through 1996. They give a mean value of 9.6°C at 1,830 m a.s.l., and a negative 6.5°C/km lapse rate was used to adjust this temperature for elevation. Well water temperatures have a wide range of values at a given elevation indicative of a multiplicity of flow paths and depths of penetration.

A base map of the study area in Fig. 6 shows five major drainages that are tributaries to Tongue Creek. Surface Creek carries about half the discharge, while the other four carry the remainder. Analyses of US Geological Survey stream hydrographs for Surface Creek and Ward Creek are shown in Fig. 7. The discharge portion of the curves exhibit two different slopes, one steep, and the other very gradual. These are interpreted as discharge from unconsolidated surface material, followed by bedrock discharge. Hydrographs for the other tributaries have the same character as those in Fig. 7. Bedrock base flows from hydrographs of the five tributaries are summarized in Table 2.

The hydrographs show that after the winter snow pack has melted the surficial material can completely discharge within a 4–6-month period. Mean annual flow of all five tributaries measured at these gauges is 2.4 m^3/s, while combined bedrock base flow totals 0.3 m^3/s. The linear precipitation model predicts that 75% of the total precipitation, or 11.3 m^3/s, falls above the average gauge elevation. This precipitation on the watershed can therefore be partitioned into roughly 18.5% alluvial discharge, 2.5% bedrock discharge, and 79% loss to evaporation, transpiration, and water flowing to lower elevation outside of the gauges. Of the 2.4 m^3/s of total discharge to the gauges, bedrock base flow accounts for 13%. Numerical simulation of groundwater flow presented below predicts the spatial distribution of discharge from bedrock as flux through the water table. According to this simulation, about 40% of the total bedrock discharge occurs above the average gauge elevation, implying that total base flow from bedrock within the study area should be 0.75 m^3/s. Mean hydraulic conductivity must be adjusted in groundwater flow and heat transport models presented below in order to match this estimated base flow.

Based upon the characteristics presented above, the relative importance of conduction and convection can be

Table 3 Finite-Difference Grid Parameters

	Distance (m)	Number of cells	Cell size (m)
X-grid (east–west)	35 km	200	175
Y-grid (north–south)	27 km	200	135
Z-grid (elevation)	3.5 km	100	35

Table 5 Specification of fault parameters

Fault block	X_1 (grid)	Y_1 (grid)	X_2 (grid)	Y_2 (grid)	Width (m)	Vertical displacement (m)
1	81	1	87	200	0	25
2	100	1	111	200	0	0
3	80	1	200	200	0	25
4	200	1	200	200	0	244

The points (X_1,Y_1) and (X_2,Y_2) are endpoints of a line along the strike of a fault plane with vertical dip

DOI 10.1007/s10040-006-0058-8

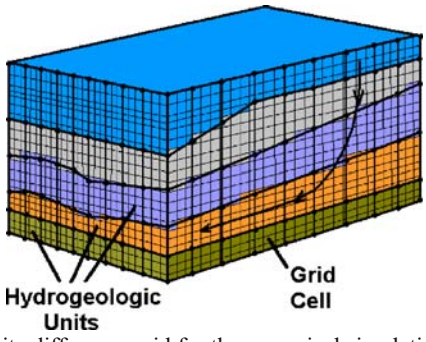

Fig. 8 Finite difference grid for the numerical simulation. The grid cells are uniform in size and hydrogeologic units cross cell layers. A hydrogeologic unit is many cells thick, which allows curved flow paths within each unit

evaluated using the two-dimensional geothermal Peclet number (Pe*; van der Kamp and Bachu 1989):

$$P_e^* = \frac{\left[(\rho c)_f Q_x A\right]}{K_T}, \qquad (1)$$

where A is the aspect ratio of the flow basin (0.1), K_T = thermal conductivity (3.3 W m^{-1} °C^{-1}), ρ = density of the fluid (998.2 kg/m^3), c = specific heat of the fluid (4186.0 J kg^{-1} °C^{-1}), and Qx = horizontal fluid flux through the system per unit width (0.75 m^3/s per 43.3 km). The factor 43.3 km is the approximate width if the concave groundwater divide were unfolded into a straight line to produce a two-dimensional flow regime. If Pe*$\gg$1, convection dominates, while for Pe*$\ll$ 1, conduction dominates. For the given values, Pe* equals 2.2 indicating that convection should be an important influence on the thermal regime of the watershed.

The geology and geomorphology of Grand Mesa have been studied for decades and have many interesting features (Yeend 1969; Young and Young 1977; Cole and Sexton 1981; Ellis et al. 1987; Dethier 2001; Cole and Aslan 2001). The site consists of Cretaceous and Tertiary formations capped by Miocene basalt flows. The oldest formation exposed is the Cretaceous Mancos Shale of marine origin, followed by the Mesaverde Group of coastal deposits laid down as the Cretaceous sea retreated from the area. This group contains the Rollins Sandstone and a sequence of up to six coal seams which are overlain by a fluvial sequence of shales and sandstones. Above the Mesaverde Group, the Tertiary Wasatch, Green River, and Uinta Formations consist of fine-grained sandstone, siltstone, and shale deposited near the margin of large lakes that served as evaporation basins. The Green River Formation in particular formed commercial deposits of nahcolite and trona north and west of the study area (Dyni 1996). Overlying these are 200 m of Miocene basalt flows that have protected the soft underlying strata from erosion. The Bureau of Reclamation (Weston 1987) conducted studies of the aquifer potential of the basalt flows on top of Grand Mesa and concluded there was insufficient water for urban use, though the basalt contained 1.39×10^8 m^3 of water with a recharge rate of 0.25 m^3/s. Hydraulic conductivity of the basalt was estimated to be 6.7×10^{-6} m/s. A potentiometric dome was found within the basalt that was 40 m higher in the center than at the edges, where the aquifer discharged to springs and seeps.

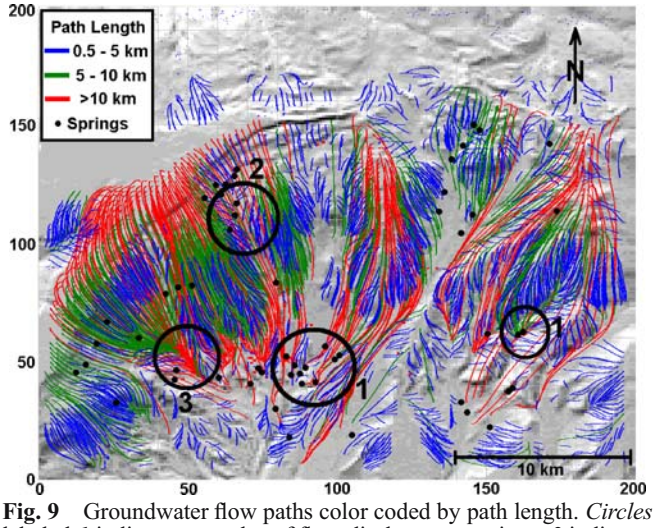

Fig. 9 Groundwater flow paths color coded by path length. *Circles* labeled *1* indicate examples of flow discharge to springs, *2* indicates shallow flow crossing over deep flow, and *3* is an example of focusing and convergence of flow from diverse pathways and depths. *Coordinates* are finite-difference grid cell numbers

During the Pleistocene, there were at least two episodes of glaciation on Grand Mesa, which formed a widespread layer of till down to an elevation of 2,300 m a.s.l. on the south flank (Yeend 1969; Hail 1972). During warming trends, glacial melt water saturated the underlying bedrock of Tertiary shale and triggered large landslides and mudflow events that carried basalt rubble across pediment surfaces at lower elevations. Where mudflows coated the bedrock surfaces with basalt debris, they were protected from further erosion and formed terraces as stream base levels steadily declined around them (Cole and Sexton 1981). The 0–60-m-thick blanket of till at high elevation serves as temporary storage for precipitation, and it is hydraulically connected to both surface streams and bedrock. At lower elevations, the deposits are discontinuous, and isolated pods serve as local aquifers for domestic water wells. For the remainder of this report these deposits of debris flows, till, and outwash will be referred to as unconsolidated surficial material, which produces the rapid discharge portion of the stream hydrographs shown in Fig. 7.

Structurally, the study area is on the southern margin of the Piceance Basin, which is a producer of natural gas and an area of active gas exploration and development. The basin center lies about 50 km north of the boundary of the study area and strata dip northward into the basin at 3–5°. Near the basin center, the Cretaceous strata are buried at over 2.5–3 km deep, have very low permeability, and are overpressured from thermogenic gas generation. Vitrinite reflectance (R_0) values for coal near the basin center exceed 1.8% R_0, indicating high thermal maturation (Kaiser and Scott 1996).

 DOI 10.1007/s10040-006-0058-8

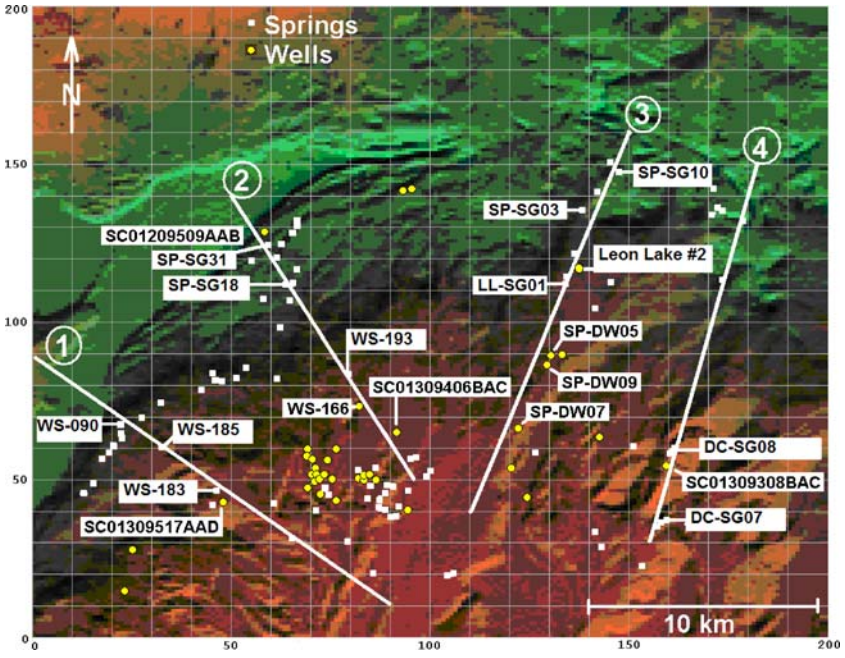

Fig. 10 Location map for cross-sections through the three-dimensional volume. The slices were chosen radially, so flow would be parallel to the plane of the section. Water wells and springs shown on cross-sections are labeled. *Coordinates* are finite-difference grid cell numbers

In contrast, these same formations within the study area have normal pressure, are water saturated, have coal vitrinite reflectance values less than 0.6% R_0, and outcrop at about 1,850 m a.s.l. Thus, strata in the study area have undergone a very different diagenesis and thermal maturation history compared to strata in the basin center. For this reason, extrapolation of data from gas wells in the basin center to the study area should be avoided.

About 20 km east of the study area, lies the West Elk coal mine and the West Elk volcanic area, consisting of Tertiary laccoliths with numerous dikes and faults (Ellis Margaret et al. 1987). This area is characterized by water-filled fractures in fault zones that are encountered by coal mines 450 m below the ground surface. These fractures produce inflows for brief periods until water in the fractures is depleted. Water temperatures are 30°C, and local thermal gradients are 70–80°C/km, or more than double that of the study area. The water has C14 age dates as old as 10,500 years. The Rollins sandstone, which underlies the coal seams, appears to be the fractured groundwater reservoir that is the source for this water (Mayo and Koontz 2000). Similar conditions were encountered in the nearby Lone Pine #1 exploratory gas well (Lat. 38.987605, Long. −107.505399, 2,427 m a.s.l.) drilled by Gunnison Energy Corporation in which water-filled fractures were encountered at depths of 564–686 m with inflows of 0.0031 m^3/s. In addition, the D-coal seam and overlying sandstone at depths between 724 and 726 m in the same well, produced flows of 0.0013 m^3/s (Wright Water Engineers, 2004, personal communication).

In contrast to the area of the West Elk mine, exploratory gas wells in the study area have not encountered water-filled fractures or significant inflows to the wells, and in general, they have very low water production rates in the range of 0–0.0005 m^3/s (Wright Water Engineers, 2004, personal communication). Likewise, abandoned coal mines within the study area experience steady discharges of groundwater with temperatures in the range of 15–20°C. (R. Klein, 2001, personal communication). This groundwater discharge is not necessarily associated with specific fractures or faults, and is not confined just to coal mines, as there are about 120 natural springs mapped within the study area over a wide range of elevation. This number is not exhaustive, since there are large areas of restricted access that have not been mapped with regard to springs.

Comparisons of the Tongue Creek watershed to surrounding areas indicate that the study area differs significantly from the center of the Piceance Basin and the coal mining areas to the east. The geologic, lithologic, and hydrological properties of surrounding areas do not provide data relevant to the study area, and extrapolation of data from those areas should be avoided. In this study, the Tongue Creek watershed is evaluated as an independent entity, and hydrological properties of the watershed are derived from local hydrological constraints and numerical simulations.

The conceptual hydrological model

Basic data used to develop a conceptual model for the hydrology of the Tongue Creek watershed have been presented above and they include precipitation rates, configuration of the water table, base flow estimates for groundwater discharge, regional heat flow, thermal gradient, and temperatures of springs and well water. The conceptual model indicated by these data includes the following features: (1) the amount of precipitation far exceeds the capacity of the ground to absorb it; (2) most precipitation runs off or is stored short term in the

 DOI 10.1007/s10040-006-0058-8

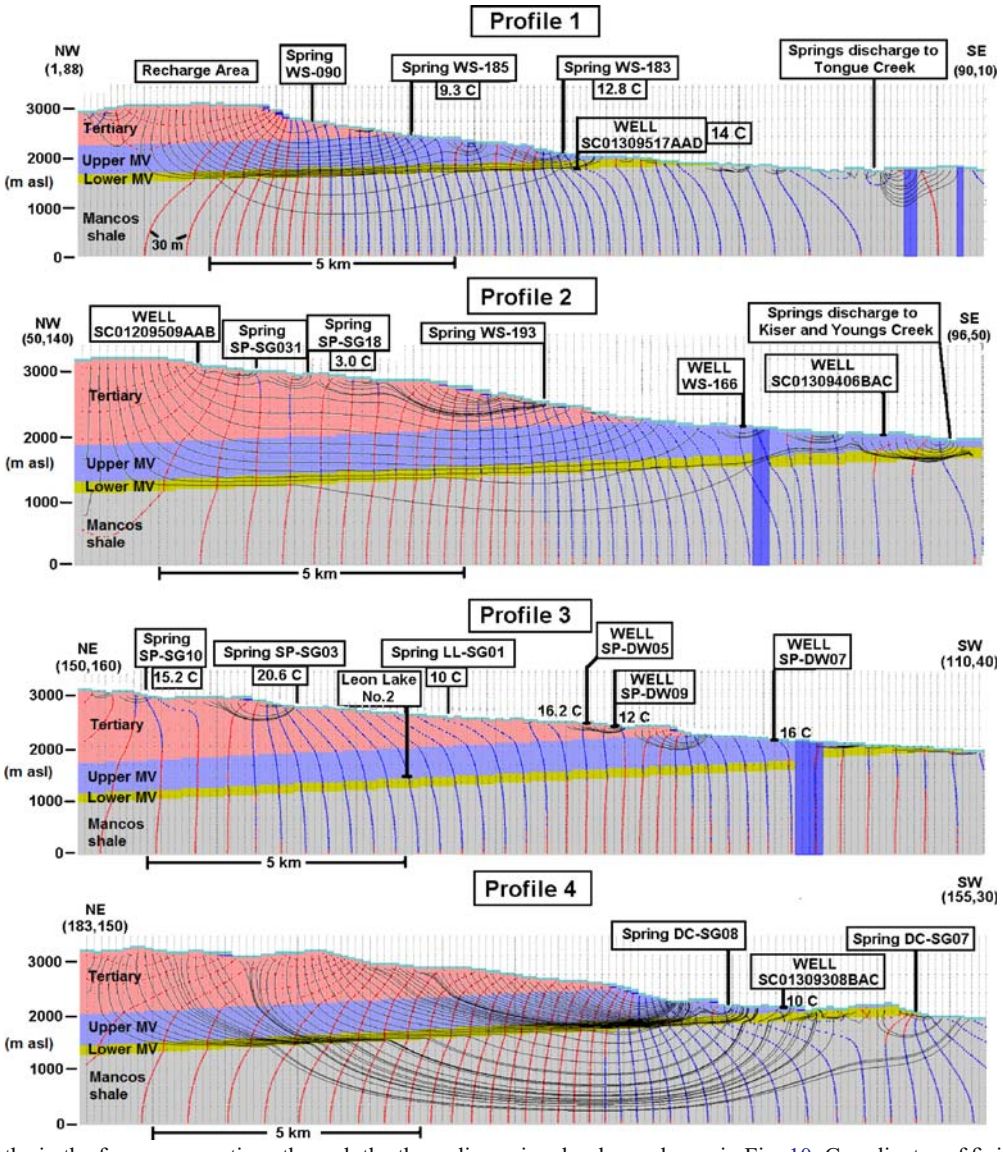

Fig. 11 Flow paths in the four cross-sections through the three-dimensional volume shown in Fig. 10. Coordinates of finite-difference grid cells are indicated at either end of each cross-section. *Color* denotes the dipping hydrogeologic units defined in Table 5 and the unconsolidated surface layer. *Heavy contours* are hydraulic head at 30-m intervals, with *red* indicating downward flow, and *blue* upward flow. The *thin black lines* are flow lines that run from *left to right* in the direction of decreasing head. The locations of springs and wells are indicated. Springs generally correspond to areas of upward flow at the water table

unconsolidated surface material as it flows toward local streams; (3) water in the surface material in flat topography is held in contact with bedrock, allowing recharge by percolation; (4) a large surface area of about 2.6×10^8 m^2 is provided for recharge by the basalt cap, glacial till, and lakes within the watershed; (5) the bedrock has low hydraulic conductivity and is saturated up to the bedrock surface; (6) groundwater flow within the unconsolidated surface layer is parallel to the surface due to the small aspect ratio of thickness to aerial coverage; (7) bedrock provides a larger aspect ratio allowing development of deep flow and arcing flow paths driven by the configuration of the water table; (8) deep groundwater flow through the high thermal gradient resulting in convective heat transport that modifies the conductive thermal regime.

Design of the numerical simulation

The objective in this study was to model the steady-state dynamic equilibrium of the hydrological and thermal systems. Under steady-state conditions, the mathematical formulation of a hydrological model is greatly simplified. The configuration of the water table is fixed and acts as a constant head surface. The temperature distribution in the subsurface is also fixed. Parameters such as specific yield and storativity associated with transient responses are not

 DOI 10.1007/s10040-006-0058-8

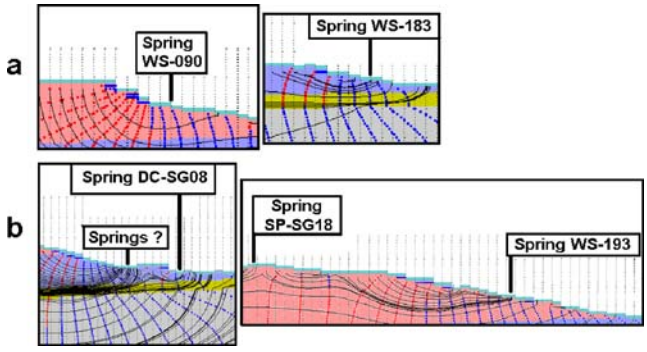

Fig. 12 Details of flow associated with spring locations. **a** Springs occur at changes in topographic slope below ridges, and **b** springs occur where flow is focused and concentrated at discharge points. See Fig. 11 for a description of features in this figure

relevant, and hydraulic conductivity is the only required parameter. All hydrogeologic units are confined since there is no drawdown or change in saturated thickness. In numerical simulations, the water table is placed at the alluvium/bedrock contact. The fixed head water table requires an exchange of flow between bedrock and the surface layer to maintain the water-table level. The surface layer can therefore be replaced by this flux, and details of flow in the unconsolidated material are not needed to account for bedrock flow. For this reason, this flow is not included in the numerical simulation, though it has a significant role in the overall hydrological system.

Mathematically, the steady-state model reduces to a boundary value problem where hydraulic head and temperature within the volume are completely determined by their values or derivatives on the boundary of the volume. Finite-difference techniques were used to solve the partial differential equations governing both groundwater flow and heat transport. For this technique, the model volume is divided into small elements of uniform size in which hydraulic head and temperature are assumed to be constant. Spatial gradients are approximated by differences in values between cells. Groundwater flow simulation was done with the MODFLOW program from the US Geological Survey, and heat transport was computed with custom code by the author.

Steady state requires that there is no net flux of water or heat into any volume element in the model. Zero net fluid flux requires the sum of the flux (Q_i) through all faces of a volume element to be zero, thus for a finite-difference cell with six faces indexed by i=1–6,

$$\sum_{i=1}^{6} Q_i = \sum_{i=1}^{6} k_i \Delta h_i = 0. \quad (2)$$

Here, k_i = hydraulic conductance (m^2/s) across the ith face, and Δh_i = change in hydraulic head (m) across the ith face.

The heat flux equation involves terms for convection, conduction, and heat from head loss along a flow path (Manga and Kirchner 2004). Groundwater flux across the ith face transports heat across the face at the rate of $\rho c_f Q_i \Delta T_i$ (W), where $(\rho c)_f$ is heat capacity of water (J m^{-3} °C^{-1}), and ΔT_i is the change in temperature of water crossing the face. The rate of heat conduction across the ith face is $k_T \Delta T_i$, where k_T is thermal conductance (W/°C), and ΔT_i is temperature difference across the face. Heat from head loss

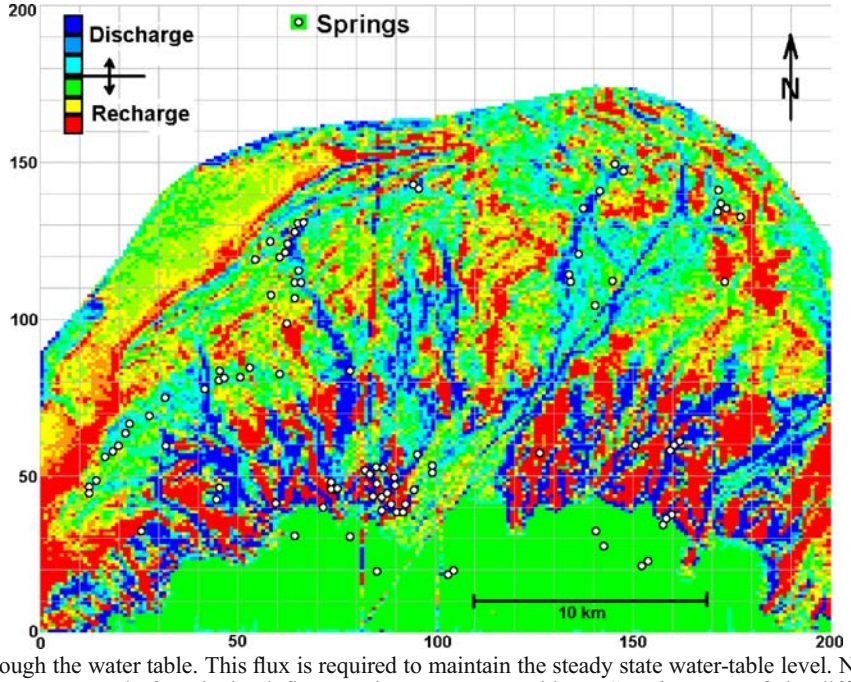

Fig. 13 Map of flux through the water table. This flux is required to maintain the steady state water-table level. Note that discharge occurs along drainages, indicating streams gain from bedrock flow. Recharge occurs on ridges. *Coordinates* are finite-difference grid cells. The *top border* is the groundwater divide. Linear features are fault traces

 DOI 10.1007/s10040-006-0058-8

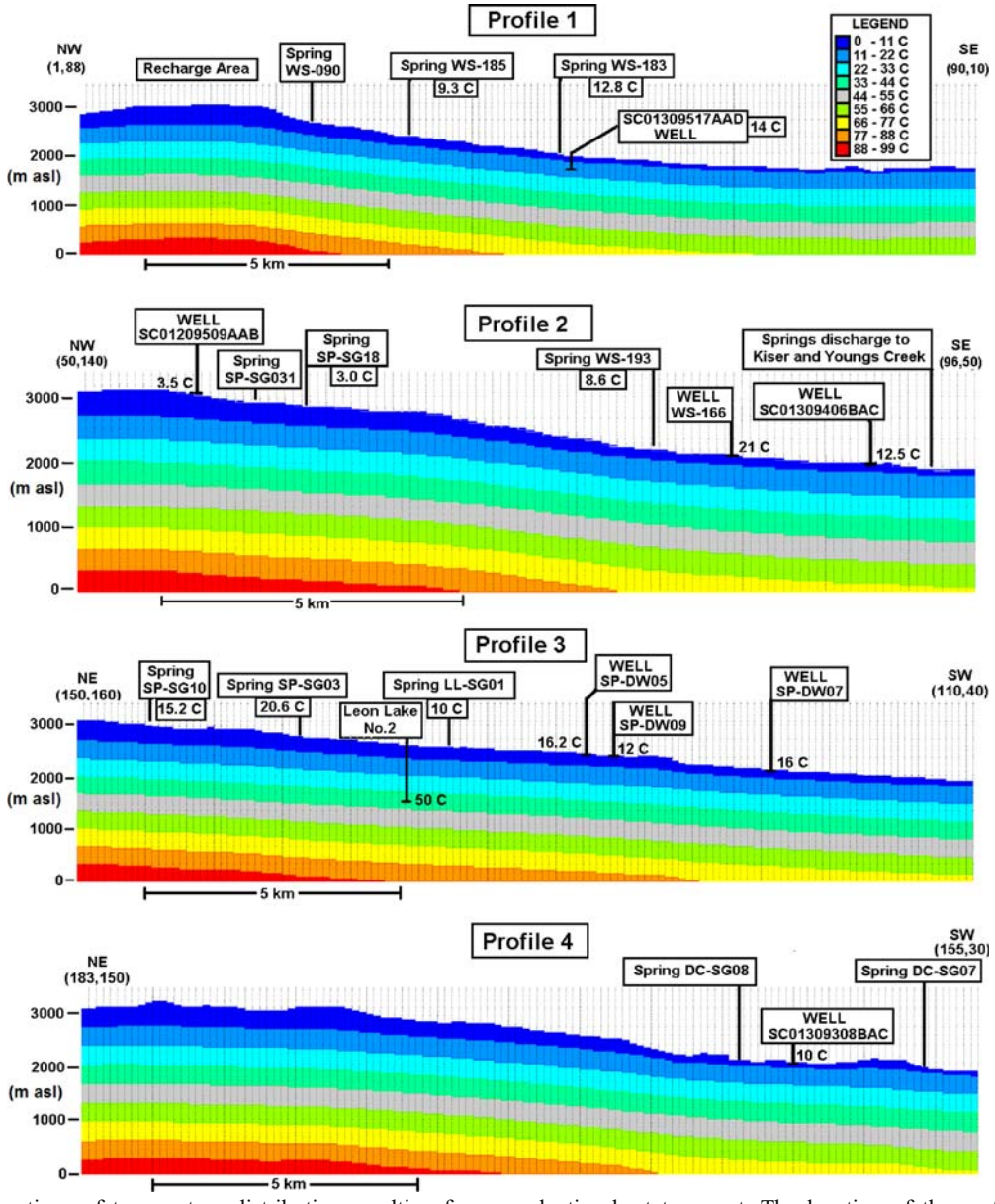

Fig. 14 Cross-sections of temperature distribution resulting from conductive heat transport. The location of the profiles is shown in Fig. 10 and coordinates of finite-difference grid cells are given at either end of each cross-section. Temperature *contours* are parallel to the ground surface and evenly spaced indicating a constant gradient. Note that the temperature in Leon Lake No. 2 on profile 3 does not agree with this model. Two spring temperatures on the *left side* of profile 3 are quite anomalous and may be influenced by ambient temperatures at the time of measurement

is released to a cell from the drop in head as water enters the cell. Combining these terms and requiring zero net heat flux to a cell gives

$$\sum_{i=1}^{6}\left[(\rho c)_f Q_i \Delta T_i\right] + \sum_{i=1}^{6}\left[k_T \Delta T_i\right] + \rho g \sum_{i=1}^{6}\left[Q_i \Delta h_i\right] = 0, \quad (3)$$

where ρg = weight per unit volume of fluid = 9.78×10^3 kg m^{-2} s^{-2}.

The relative contribution of the three mechanisms of heat transport in Eq. (3) can be seen from their ratios. Define A = convection, C = conduction, and H = heat from head loss, and assume effects from convection are small so conduction is nearly vertical. Then

$$C = k_T[\Delta T]_z \quad (4)$$

and the ratio of A/C for vertical flow can be written as

$$A/C = \frac{\left[(\rho c)_f K_H [\nabla h]_z \Delta z\right]}{K_T}, \quad (5)$$

 DOI 10.1007/s10040-006-0058-8

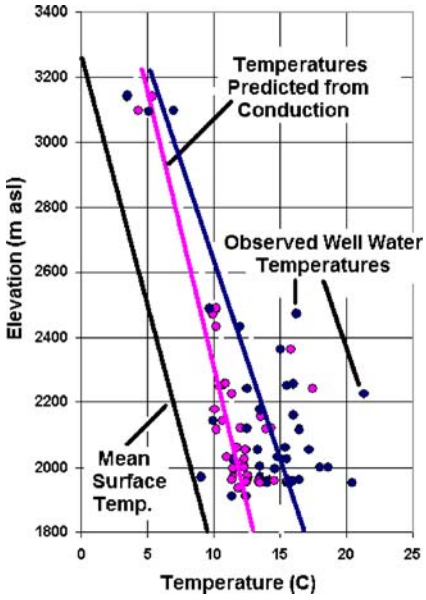

Fig. 15 Predicted well-water temperatures from the conductive heat flow model (*pink*) vs. observed well-water temperature (*blue*) as a function of elevation. Conductive flow produces very low scatter and lower than average observed temperatures at low elevation

where subscript z denotes the vertical component of the gradient of hydraulic head, Δz is the vertical cell dimension, and K_T is thermal conductivity (W m^{-1} $°C^{-1}$). For hydraulic conductivity $K_H=10^{-8}$ m/s and hydraulic gradient of 0.25, the ratio of vertical convective flux to vertical conductive flux would equal 0.1, and for $K_H=10^{-7}$ m/s, the ratio would be 1.0.

Likewise the ratio of H/C for vertical flow is

$$H/C = \frac{[\rho g K_H \nabla h^2 \Delta z]}{K_T \nabla T} \quad (6)$$

Using a hydraulic gradient of 0.25 and $K_H=10^{-8}$ m/s, this ratio equals 0.0021. This is a factor of 50 times smaller than the influence of convection, so heat from head loss is a small factor in the heat balance for vertical flow at this site. Manga and Kirchner (2004) found that the contribution of heat from gravitational potential energy was significant for cold springs if discharge rates are high. They also found that spring temperatures exceed surface temperatures only for low flux rates and deep penetration. Here the total flux through the bedrock is small, so the heat contribution from head loss is diminished. The fact that groundwater temperatures exceed surface temperatures by up to 15°C indicates deep flow in this study area.

For convenience, the fixed water table was located one grid cell below the ground surface. Thermal conductivity of the surface cell was set to one-half the value in the saturated zone to simulate unsaturated surface material (Clauser and Huenges 1995). Finite-difference grid parameters for the model are given in Table 3, and initial hydraulic conductivities for hydrogeologic units are given in Table 4. These conductivities were chosen to represent relative values between hydrogeologic units based upon their lithology. The absolute scale for conductivity is derived below using linear properties of the model by matching model output to estimated base flow. Table 5 contains specification parameters for fault planes incorporated into the model. Hydrogeologic units do not correspond to grid layers in this model as is common in MODFLOW usage. Instead, grid cells are uniform in size and hydrogeologic units may cross grid layer boundaries and may be many grid cells thick. This specification allows curvature of flow paths within each hydrogeologic unit, which is necessary for accurate numerical simulation. This concept is illustrated in Fig. 8.

Fluid flow boundary conditions for the model prevent flow through the bottom or sides of the volume, and maintain a fixed head at the water table equal to the water table elevation. Thermal boundary conditions prevent flow through the sides of the volume, and used a constant heat flow through the bottom of the model of 100 mW/m^2 defined by setting the gradient at the lower boundary to 0.03°C/m. The temperature at the ground surface was set equal to the mean surface temperature estimated from mean daily temperatures at Cedaredge, Colorado (1,830 m a.s.l.) between 1977 and 1993. This value of 9.6°C was extrapolated as a function of elevation, using a lapse rate of −6.5°C/km of elevation. This boundary condition is somewhat restrictive on the solution since the presence of convective heat transport modifies the surface temperature distribution, but this is not addressed in this model.

Smith and Chapman (1983) pointed out the importance of temperature effects on density and viscosity. Most groundwater flux in the study area occurs within a thermal range from 0 to 50°C. Over this temperature range, the density of water varies by less than 1% so buoyancy effects are neglected. Viscosity of water decreases by a factor of 3 over this same range which increases hydraulic conductivity by the same factor. Dependence of viscosity on temperature is ignored in the numerical simulations, so estimates of hydraulic conductivity from thermal constraints may not reflect properties of the lithology alone.

Simulation results for groundwater flow

Groundwater flow and heat transport solutions were done independently, so the distribution of hydraulic head computed by MODFLOW was held constant during heat transport simulation. The solution for groundwater flow converged with a maximum residual error in hydraulic head of 0.6×10^{-5} m and a water table flux (bedrock base flow) of 0.63 m^3/s. The ratio of estimated base flow for the watershed of 0.75 m^3/s to the modeled base flow of 0.63 m^3/s indicates that the initial guess for hydraulic conductivities is too low and must be multiplied by a factor of 1.2.

Two display modes are used to visualize groundwater flow in the three-dimensional volume, one being a plane-view map of flow paths, and the other being cross-sections

 DOI 10.1007/s10040-006-0058-8

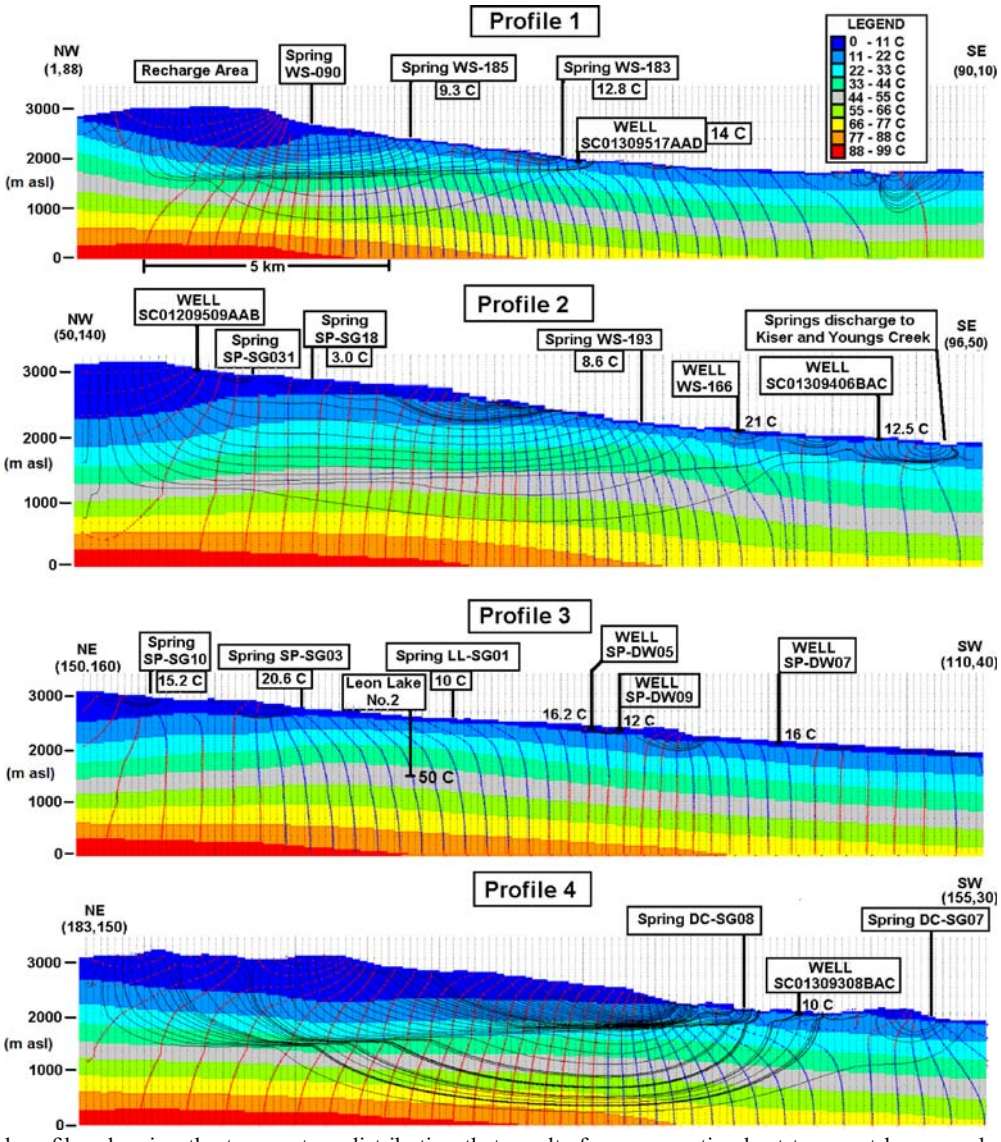

Fig. 16 Selected profiles showing the temperature distribution that results from convective heat transport by groundwater. Comparison with Fig. 14 shows suppression of temperature under recharge areas and elevation of temperature in discharge areas. Note that the temperature in the *Leon Lake No. 2 well* is now in close agreement with the predicted temperature

through the volume. For the display in Fig. 9, flow paths have been traced for elements of water starting at the water-table surface in areas of downward flow. The paths are followed along the negative gradient of head until they again reach the surface. The length of a path is color coded with red for long deep paths and blue for shallow short paths. This plane view shows a number of interesting features. In general, the shallow (short) paths are influenced by local topographic gradients and flow down slope toward the nearest drainage. Long paths penetrate to depths of several kilometers and are influenced by large-scale topographic features such as large ridgelines. Circle 2 shows an area where shallow flow crosses over deep flow due to their differing influences. Circles labeled 1 are areas where flow paths converge toward discharge to springs. In many cases, paths of differing lengths converge to the same discharge areas where they may mix with each other, and with alluvial water, to form a wide variety of water chemistries and temperatures. However, analysis of water chemistry is beyond the scope of this report. The circle labeled 3 shows an example of focusing and convergence of flow from a wide area, and a wide range of path lengths, into a small discharge area. Several of the converging flow lines in Fig. 9 appear to be directly associated with particular springs. It is evident that springs in proximity to each other may have very different source areas in this three-dimensional geometry.

There are two areas in this display that are devoid of flow paths. Flow originating at the surface does not pass through these regions of the model. One is a strip in the center, and the other is to the right of center. This results

 DOI 10.1007/s10040-006-0058-8

from diversion of flow around these valleys by hydraulic gradients generated by the topography of the water table. Since strata dip gently north and strike west, all curvature of flow is controlled by the water table rather than lithology.

Four vertical cross-sections through the three-dimensional volume were taken in radial directions, so that flow is mostly parallel to the plane of the section. The location of these profiles is shown in Fig. 10, and Fig. 11 shows a comparison of the four sections. Heavy lines are contours of constant hydraulic head at 30-m intervals. Where flow is downward, the contours are red, and where flow is upward, they are blue. Contours are normal to grid boundaries due to impermeable boundary conditions. The thin lines in Fig. 11 running perpendicular to the contours of constant head are flow paths traced within the two-dimensional plane of the section. They provide a visualization for flow taking place within the section, but actual three-dimensional flow paths do not remain within the plane of the profile.

Some of the features seen in Fig. 11 are similar to those seen in plane view, including divergence of flow in recharge areas under topographic highs, and convergence of flow into discharge points under topographic lows. Flow from diverse source areas may be focused and channeled into a common discharge region by gradients produced by the water-table topography.

The displays show that springs occur at the base of slopes where topography flattens out, since this induces arcing flow paths in the shallow groundwater. Springs also occur where flow paths are focused and converge to form concentrated flow to the surface. Detailed displays of flow patterns associated with mapped springs are shown in Fig. 12. Nearly all mapped springs are associated with increased upward flow at the water table in the numerical solution, and there are other locations with the same characteristics where no mapped spring is indicated. These are often in areas of restricted access where the existence of a spring cannot be verified.

As mentioned previously, the steady-state water table requires a flux through the water-table surface at every point to maintain the constant water level. Figure 13 is a color-coded flux map of the water table in which recharge areas are red, and discharge areas are blue. Recharge occurs on topographic highs, and discharge occurs in topographic lows, particularly into streams and springs. This flux map illustrates the high correlation between predicted discharge areas and the presence of springs, and it shows that most streams gain flow from bedrock along their course. Hydrographs in Fig. 7 show that the discharge of bedrock water to streams is small compared to their average volume of flow.

Simulation results for convective heat transport

The groundwater flow solution discussed in the previous section was used as input to the heat transport program. Two heat-flow solutions were computed for this model, one for conduction alone, and the second incorporating conduction, convection, and heat from head loss. Both solutions were iterated until the maximum residual error was less than 10^{-3}°C. The same four cross-sections shown in Fig. 11 were extracted from the three-dimensional temperature volume for each solution. The conductive solution is displayed in Fig. 14 and illustrates the distribution of temperature expected from the interaction of regional heat flow with local topography in the absence of groundwater flow. Figure 15 compares temperatures extracted from the solution at the location and depth of water wells with observed water temperatures from Fig. 5. The black line represents the mean surface temperature as a function of elevation, pink symbols are model temperatures, and blue symbols are observed temperatures. The root mean squared (RMS) error between observed and predicted temperatures is 5.0°C. The high regional heat flow accounts for some of the observed temperature anomalies at low elevations, and most of the anomalies at high elevations.

The solution that incorporates convection, conduction, and heat from head loss is shown in Fig. 16. This solution exhibits significant perturbations to the thermal regime. Temperatures are suppressed under recharge areas and elevated at discharge points. Extracted water temperatures at well locations displayed in Fig. 17 show a significant shift in the distribution of temperature with elevation that matches the observed distribution fairly well. The RMS

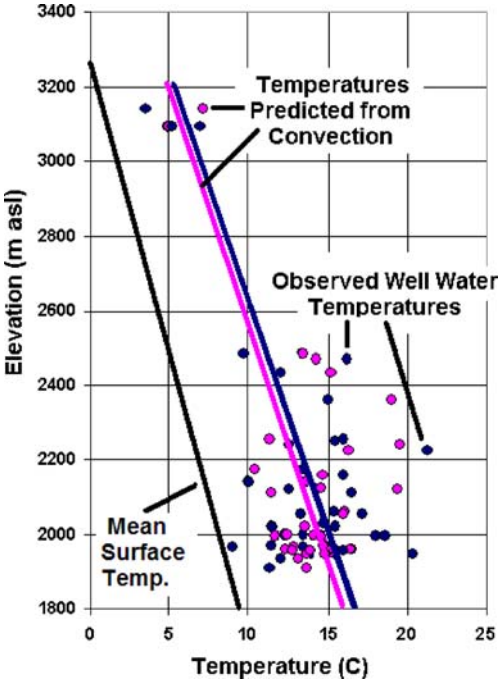

Fig. 17 Observed well-water temperature data (*blue*) compared with predicted well-water temperatures from the convective heat transport model (*pink*). The *black line* is mean surface temperature with a lapse rate of −6.5°C/km of elevation. The convective heat transport model predicts greater scatter in temperatures at a given elevation than the conduction model due to three-dimensional variability of flow paths and variable depths of penetration, and fits the trend of groundwater temperature with elevation

 DOI 10.1007/s10040-006-0058-8

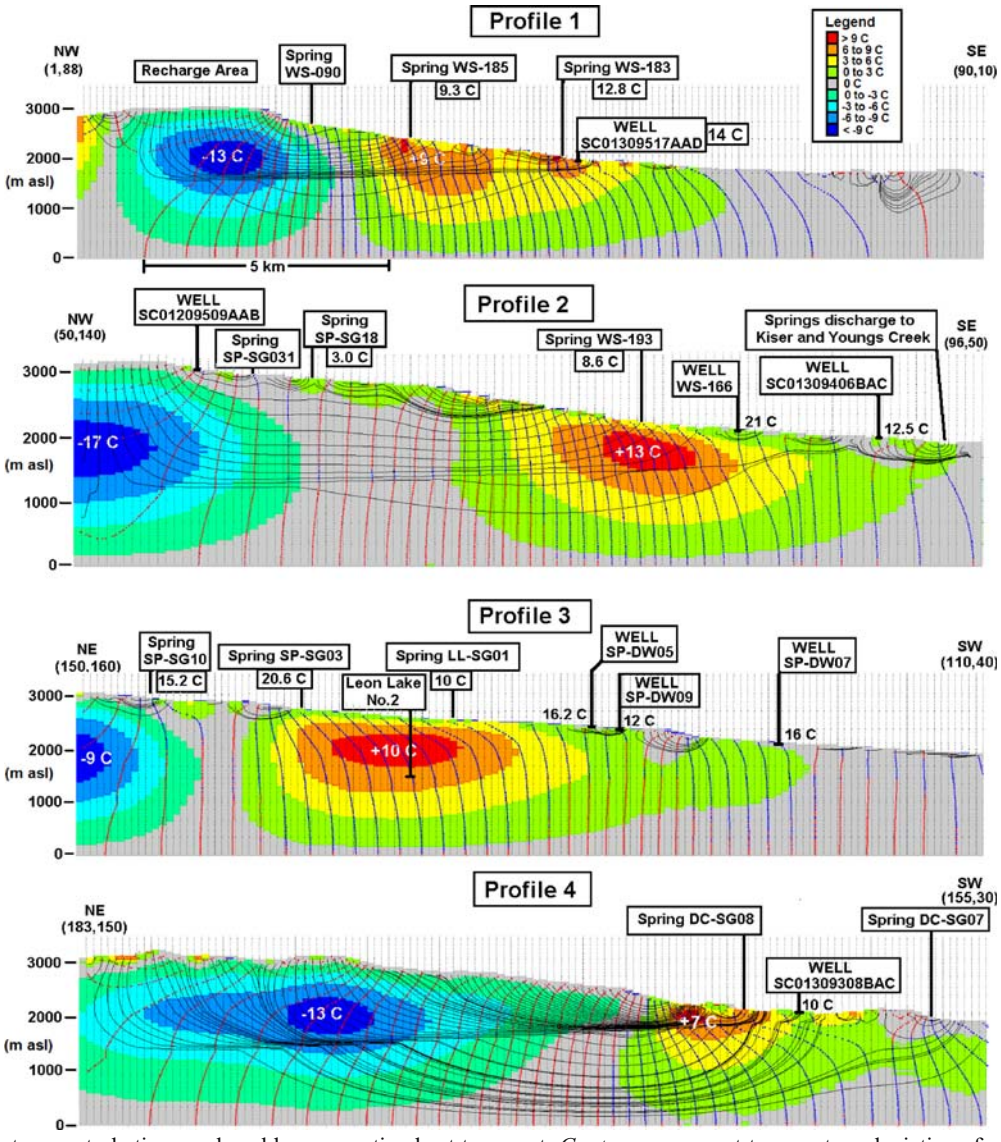

Fig. 18 Temperature perturbation produced by convective heat transport. *Contours* represent temperature deviations from the conductive solution shown in Fig. 14 that result from convective heat transport

error between observed and predicted temperature in this model is 3.04°C.

Figure 18 shows the difference between the temperature distribution for convective and conductive heat transport. The temperature anomalies are areas where convection significantly modified the thermal regime.

Several factors preclude matching of individual temperature measurements. A minor factor is uncertainty in the screened interval or depth where the water originates in a well, and the degree of mixing of multiple producing intervals. More important is model uncertainty that results from using a constant depth water table. Not honoring details of water table depth influences groundwater flow and convection, as well as heat conduction through the unsaturated zone between the water table and surface boundary condition. This will introduce errors in local temperature estimates. Other factors include errors resulting from discretization of the finite-difference grid, and variability in hydraulic and thermal conductivity within the site. Detailed information would be required to improve the model accuracy for specific data points.

The scale of hydraulic conductivity has been constrained by the base flow of the watershed, and the match of predicted and observed temperature distributions provides a consistency check on the hydrological model. Woodbury and Smith (1988) also found that incorporation of thermal data aided estimation of hydraulic conductivity, and it is interesting to note that the values of their parameters for the Downie Slide in British Columbia were very similar to those for this study area.

Hydraulic conductivity has been isotropic in all numerical simulations presented above. Introduction of anisotropy, where horizontal conductivity exceeds vertical

 DOI 10.1007/s10040-006-0058-8

conductivity, produces several adverse effects in the models, even for relatively low values. These effects include the disappearance of upward flow at the location of mapped springs, and diminished thermal perturbations which result from reduced depth of penetration (Smith and Chapman 1983). In addition, the scale of hydraulic conductivity of 10^{-8} m/s is perhaps two orders of magnitude higher than expected for clay rich lithology (Hornberger et al. 1998). This combination of factors suggests that fracturing has enhanced vertical conductivity and eliminated the anisotropy that would normally be expected for this lithology.

Conclusions

Several independent steps have led to numerical simulations of groundwater flow and heat transport that appear to explain the distribution of observed water temperature data, location and source of springs, bedrock base flow, and the geometry of groundwater flow in the study area. The steps included the use of thermal conductivity, heat flow, and thermal gradients from oil and gas wells to model the distribution of subsurface temperature, and the use of numerical simulations of groundwater flow to derive the scale of hydraulic conductivity from estimated base flow of the watershed. The latter, in turn, depended upon the assumption that the water table follows surface topography throughout the site, and was based upon measurements in a limited portion of the area. All of these factors affect the balance between convection and conduction, and the degree of perturbation of the thermal regime that leads to observed groundwater temperatures.

Internal consistency between the thermal and hydrological models provides evidence for the existence of deep groundwater flow in the study area. A non-uniqueness lies in the assumption of a constant thermal conductivity and uniform heat flow across the area. It is possible that the observed distribution of groundwater temperatures could be explained by a specific combination of thermal conductivity and heat flux rather than convective heat transport. Therefore, the observed temperature distribution of groundwater is evidence for the existence of deep groundwater flow under the assumption that there are no other sources of heat flow variation across the study area.

Acknowledgements This work was done without financial support of any kind, purely to satisfy scientific curiosity. Thanks to my wife, Dr. Frances P. Lazear, for many helpful discussions, reviews of this work, and for moral support during several years of research. Thanks to State Water Commissioner Steve Tuck for guidance to numerous remote springs west of Cedaredge on several day-long horseback rides, and for historical information regarding these springs based upon his 30 years as commissioner and 50 years of riding through the country. Thanks also to Mr. Wayne Wolf for guidance and access to springs in the Currant Creek and Dry Creek canyons of the study area, and for supplying 4-wheelers for transportation into the remote country. The author had many helpful discussions with T. Cort, R. Cole, A. Trevena, and G.A. Miller. Thanks to W. Hood, F. Lazear, R. Flinn, A. Trevena, and C. Graff for critical reviews of drafts of this research. Thanks also to the reviewers for many good suggestions that have greatly improved this final manuscript.

References

Anderson MP (2005) Heat as a ground water tracer. Ground Water 43(6):951–968

Brooks T, Ackerman DJ (1985) Reconnaissance of ground water resources in the lower Gunnison River basin, Southwestern Colorado. Water-Resources Investigations Report 84–4185, US Geological Survey, Lakewood, CO

Clauser C, Huenges E (1995) Thermal conductivity of rocks and minerals. AGU, Washington, DC

Cole RD, Sexton JL (1981) Pleistocene surficial deposits of the Grand Mesa area, Colorado. New Mexico Geol. Soc. Guidebook, 32nd Field Conference, Western Slope Colorado, New Mexico Geol. Soc., Albuquerque, NM

Cole RD, Aslan A (2001) Late Cenozoic erosional evolution of Grand Mesa, western Colorado (abstract). Geological Society of America Program with Abstracts (Rocky Mountain Section meeting), GSA, Boulder, CO

Deming D (1993) Regional permeability estimates from investigations of coupled heat and groundwater flow, North Slope of Alaska. J Geophys Res 98(B9):16271–16288

Dethier DP (2001) Pleistocene incision rates in the western United States calibrated using Lava Creek B tephra. Geology 29:783–786

Domenico PA, Palciauskas VV (1973) Theoretical analysis of forced convective heat transfer in regional groundwater flow. Geol Soc Am Bull 84:3803–3814

Dyni JR (1996) Sodium carbonate resources of the Green River Formation. US Geological Survey Open-File Report 96–729, USGS, Lakewood, CO

Ellis Margaret S, Gaskill David L, Dunrud C Richard (1987) Geologic map of the Paonia and Gunnison area, Delta and Gunnison Counties, Colorado. Map C-109, 1987, USGS, Lakewood, CO

Forster C, Smith L (1989) The influence of groundwater flow on thermal regimes in mountainous terrain: a model study. J Geophys Res 97(B7):9439–9451

Hail WJ Jr (1972) Reconnaissance geologic map of the Cedaredge area, Delta County, Colorado. US Geological Survey miscellaneous geologic investigations Map I-697, USGS, Lakewood, CO

Hornberger GM, Raffensperger JP, Wiberg PL, Eshleman KN (1998) Elements of Physical Hydrology. Johns Hopkins University Press, Baltimore, MD

Kaiser WR, Scott AD (1996) Geologic and hydrologic controls critical to coal bed methane reducibility and resource assessment: Williams Fork formation, Piceance Basin, northwest Colorado. GRI-95/0532 Topical Report, Gas Research Institute, Stanford, CA

Manga M, Kirchner J (2004) Interpreting the temperature of water at cold springs and the importance of gravitational potential energy. Water Resour Res 40, DOI:10.1029/2003WR002905

Mayo AL, Koontz W (2000) Fracture flow and groundwater compartmentalization in the Rollins Sandstone, Lower Mesaverde Group, Colorado, USA. Hydrogeol J 8:430–446

Smith L, Chapman DS (1983) On the thermal effects of groundwater flow. 1. Regional scale systems. J Geophys Res 88(B1):593–608

SMU Geothermal Lab Website (2004) Geothermal Map of the United States. http://www.SMU.edu/geothermal/. Cited 13 August 2005

Toth JA (1962) A theory of groundwater motion in small drainage basins in central Alberta, Canada. J Geophys Res 67(11):4375–4387

Toth JA (1963) A theoretical analysis of groundwater flow in small drainage basins. J Geophys Res 68(16):4795–4811

van der Kamp G, Bachu S (1989) Use of dimensional analysis in the study of thermal effects of various hydrogeological regimes. In: Beck AE, Garven G, Stegena L (ed) Hydrogeological regimes and their subsurface thermal effects. Am Geophys Union Geophys Monogr 47(2)

Weston LK (1987) Mesa-Delta municipal and industrial ground water study. Technical Appendix, US Bureau of Reclamation, Washington, DC

Woodbury AP, Smith L (1988) Simultaneous inversion of hydrogeologic and thermal data. 2. Incorporation of thermal data. Water Res Res 24:356–372

Yeend WE (1969) Quaternary geology of the Grand and Battlement Mesas area, Colorado. US Geol Surv Prof Pap 617:50

Young RG, Young JW (1977) Colorado west: land of geology and wildflowers. Wheelwright, San Francisco, CA, p 239

 DOI 10.1007/s10040-006-0058-8